Soft Matter

Thermophoresis of Colloids in Nematic Liquid Crystal

Journal:	*Soft Matter*
Manuscript ID	SM-ART-12-2019-002424.R1
Article Type:	Paper
Date Submitted by the Author:	21-Jan-2020
Complete List of Authors:	Kołacz, Jakub; US Naval Research Laboratory, Center for Bio/Molecular Science and Engineering Konya, Andrew; remesh Inc. Selinger, Robin; Kent State University, Liquid Crystal Institute Wei, Qi-Huo; Kent State University, Liquid Crystal Institute

Soft Matter

ARTICLE

Thermophoresis of Colloids in Nematic Liquid Crystal

Jakub Kołacz[1,2,*], Andrew Konya[1,3], Robin L. B. Selinger[1] and Qi-Huo Wei[1,*]

Received 00th January 20xx,
Accepted 00th January 20xx

DOI: 10.1039/x0xx00000x

www.rsc.org/

Thermophoresis, or the directional motion of colloidal particles in liquids driven by a temperature gradient, is of both fundamental interest and practical use. In this work we explore the thermophoresis of colloids suspended in nematic liquid crystals (LCs). We observe that the motion of these colloids is fundamentally different from that in isotropic systems as a result of elastic distortions in the director fields caused by the colloidal inclusions. In the case of a sufficiently large local temperature and gradient, the elastic energy drives negative thermophoresis of immersed particles, which has a strongly nonlinear dependence on temperature. We develop a theory that incoporates elastic energy minimization into the traditional thermophoretic formulation and demonstrated a good agreement with experimental observations. We also examine the temperature dependence of the effective viscosity of the colloids and highlight the large magnitude of the Soret coefficient ($|S_T|>5000$), which results from the inherent enhancement in thermophoresis due to elastophoretic considerations and supression of Brownian diffusion in LC media.

1 Introduction

When subject to a temperature gradient, micro-particles suspended in isotropic fluids undergo directional motion down the thermal gradient, a phenomenon widely known as thermophoresis. Thermophoresis in gases is a result of anisotropic momentum transfer between the gas molecules and the particles.[1] Thermophoresis in liquids is known to be notoriously difficult to characterize because in addition to the anisotropic momentum transfer, various temperature dependent physical properties, such as density,[2] solvation entropy,[3] and the surface charges of the colloids,[4,5] play a role.

There are two primary physical mechanisms behind thermophoresis in liquids, which stem from hydrodynamic and thermodynamic origins.[6] In the hydrodynamic case, the anisotropic local environment around the particle due to a thermal gradient leads to an imbalanced effective force on the particle. In the second case, the local environment is isotropic and in thermal equilibrium, and the particle undergoes isotropic Brownian motion which is biased over time to thermodynamically favorable regions. The relative importance of these two mechanism is determined by the two time scales that the particle needs to Brownian diffuse or directionally (thermophoretically) move a distance of its radius.[6] Most colloidal systems exhibit positive thermophoresis, where particles move from hot to cold regimes.[6,7] However, there exist circumstances where negative thermophoresis is possible, such as in multi-solvent mixtures[8,9] or when there is a nontrivial temperature dependence of physical properties such as density[7] or hydrophobicity.[10]

The net flow of colloids due to thermophoretic phenomena is quantified using the thermal diffusion coefficient D_T and the diffusion coefficient D of the particle[11,12]

$$J = -D\nabla c - cD_T\nabla T \quad (1)$$

The thermal diffusion coefficient is the ratio between the velocity of the thermophoretic motion and the temperature gradient, i.e. $D_T \equiv -v/\nabla T$. The diffusion coefficient of a spherical particle with radius R is related to the temperature T and the liquid viscosity η through the Stokes-Einstein relation: $D = k_B T/6\pi\eta R$, where k_B is the Boltzmann constant. Using Eq 1 with a zero flux, a steady state solution can be reached that expressly quantifies the thermophoretic motion using the Soret coefficient, $S_T = D_T/D$. The sign of the Soret coefficient determines the direction of motion ($S_T > 0$ is positive thermophoresis), while the magnitude dictates how distinguishable the motion is from thermal diffusion.

Thermophoresis is not only of fundamental interest, but also of practical use.[13–18] For example, thermophoresis in gasses has been widely utilized in commercial precipitators to filter fine particles from gas steams.[1] Thermophoresis in liquids is exploited as an alternative avenue to directing colloidal assembly,[19] and for sorting and characterizing polymers and biomolecules as shown

[1]Advanced Materials and Liquid Crystal Institute at Kent State University, Kent OH 44240, USA
[2]Currently at the US Naval Research Lab, Washington DC 20375, USA
[3]Currently at remesh Inc., New York NY 10010, USA
*Corresponding authors: jakub.kolacz@nrl.navy.mil, qwei@kent.edu

in Thermal Field-Flow Fractionation[13–15] and MicroScale Thermophoresis.[16–18] There is also interest in incorporating thermophoresis into microfluidic systems for potential applications in characterization and separation in lab-on-a-chip systems.[20]

One class of fluidic media that remains unexplored within the framework of thermophoresis is anisotropic liquid such as nematic LCs. Since the constituent molecules of nematic LCs possess long-range orientational order, the introduction of colloidal particles results in distortions of the director field and the formation of topological defects to satisfy the anchoring conditions set by the colloidal particle surfaces.[21] It is well known that the elastic distortion of the director field can lead to many interesting phenomena,[22] such as long-range interactions between the colloids and interfaces,[23] nonlinear Stokes drag,[24–30] nonlinear electrophoresis,[31,32] colloidal transport and self-assembly.[22] Focused laser beams can also be utilized for manipulating and transporting molecules and particles, creating gradients of the elastic energy by both local heating and optical reorientation.[33–37] How the elastic energy in LCs qualitatively and quantitatively alters the thermophoretic processes is not only a fundamental question but is also of importance to potential applications such as particle assembly and sorting.

In this work, we study thermophoresis of colloidal particles suspended in a nematic LC. First, we observe that a temperature gradient across a nematic LC can induce negative thermophoresis. We develop a theory incorporating the minimization of the Frank elastic free energy into an expression for the thermophoretic force and find good agreement with experimental observations. Finally, we examine the temperature dependence of Brownian diffusion and thermophoretic force and show the resulting large magnitude of the Soret coefficient.

2 Experimental

2.1 Materials

4-cyano-4'-pentylbiphenyl, or 5CB, is used as the nematic LC medium in our studies. 5CB has a nematic phase between 24°C and 35°C. 85 wt% glycol in water is used as the isotropic medium. From literature, we determined that the 85/15 weight ratio gives a viscosity of 75cP at 26°C,[38] which matches that of 5CB at room temperature.

Colloids used in this study are silica beads (Bangs Labs) with diameters of 1.6μm and 5μm. For LC studies, the 5μm beads are functionalized using Dimethyloctadecyl [3-(trimethoxysilyl) propyl] ammonium chloride (DMOAP), which covalently binds to the surface groups and induces homeotropic alignment of the 5CB. The concentration was less than 1×10^{-7} colloids per gram.

2.2 Experimental Setup

Samples are made of two parallel glass plates with the cell gap thickness set by 25 μm fiber spacers. Before assembly of the LC cells, the glass slides are spin-coated with thin films of the polyimide Pyralin PI2555 (HD MicroSystems), and then mechanically rubbed to induce planar alignment of 5CB along the *x*-axis (Fig 1a). Cells are assembled with antiparallel alignment in a pi-cell configuration to push the colloids into the bulk of the LC.

A stage was designed and built to simultaneously heat and cool opposite sides of a sample. Peltier elements connected in series on opposite sides of the stage ensure that the sample is exposed to the same temperature from above and below. The wiring of the positive and negative leads to the p- and n-sides of the thermoelectric elements is shown in Figure 1a. Thin copper plates fitted with thermocouples are positioned between the Peltier elements and the LC samples for uniform heating/cooling and temperature readouts. A photo of the heat stage in the optical microscope setup is shown in Fig 1b. To remain consistent with the literature definition of positive thermophoresis, the x-axis is set to point from hot to cold.

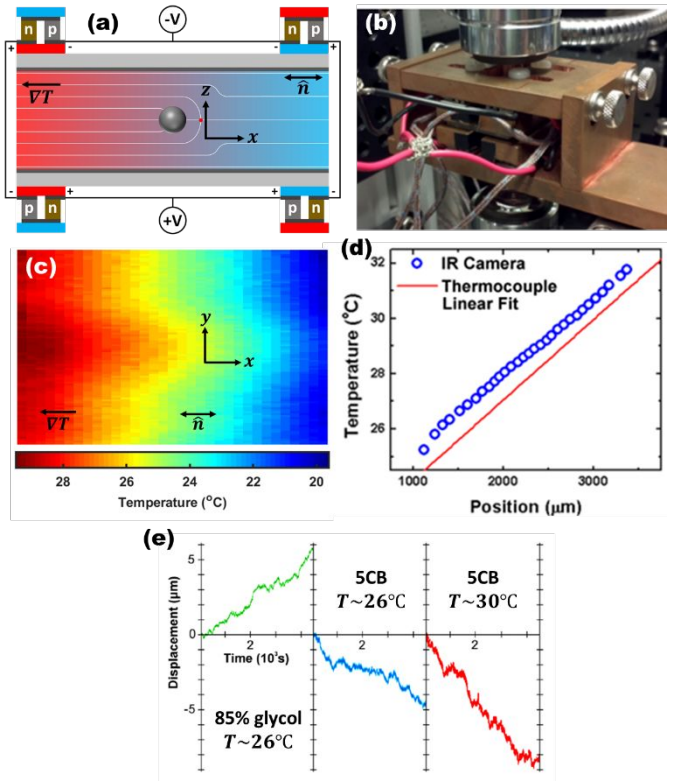

Figure 1 Experimental setup. (a) Vertical cross-section of the experimental setup: by appropriately connecting thermoelectric elements it is possible to simultaneous heat one side of the stage while cooling the other. The temperature gradient was applied along the nematic director and the negative x-axis. The black sphere represents the colloidal inclusion, which white lines showing the local director field and the red dot representing the accompanying hyperbolic hedgehog. (b) The stage positioned in the optical microscope setup. (c) An IR camera image of the top glass of the sample shows the temperature distribution of the surface. (d) The temperature gradient approximated using a linear fit from measured thermocouple values shown in red were converted into a local temperature using the results of the IR camera images, which are shown in blue. (e) Trajectories of 5μm uncoated Silica colloids in an isotropic (85% glycol) and anisotropic medium (5CB).

For LC samples, the temperature gradient is parallel to the rubbing direction of the polyimide surface, and thus along the LC nematic director $\hat{n}$. The correlation between the local temperature in the samples and the thermocouple readouts is determined by thermally imaging the sample surface (Micro-Epsilon ThermalIMAGER TIM 200) at a given gradient. A representative thermal image is shown in Fig 1c. The gradient of the temperature in the middle regions between the heating and cooling elements is approximately linear and agrees with that obtained from thermocouple readings. A temperature correlation curve (Fig 1d) is used to generate a generalized function that takes into account the thermocouple readings and the position in the sample to give an accurate reading of the local temperature.

Images of the sample are acquired and processed in LabVIEW for real-time tracking of the colloidal particles. Data collection is initiated when a colloid is centered in the microscope's field of view using a micro-positioning stage. The field of view of the optical microscopic setup with a 40x objective is about 80µm x 80µm. Due to the strong interaction between colloids, a concentration of colloids was selected to ensure an average of 1 colloid per field of view. Before the colloid moves out of view, the tracking program is stopped, the microscope stage is moved to re-center the colloidal particle, and the data collection is reinitiated. The total displacement, stitched together from the individual data sets, is shown in Fig 2a. From the temperature-position curve (Fig 1c) and the thermocouple readings, we determine the temperature gradient at each point.

3 Experimental Results

3.1 Control Experiment with Isotropic Liquid

As a control experiment to eliminate the possible effects of thermal convection, 5µm silica beads were immersed in *85%* glycerol in water. With an applied temperature gradient of *1°C/mm*, positive thermophoresis was observed with the particle velocities *~10 µm/hr*. These values are consistent in both the warm and cool areas of the sample.

Silica beads from the same batch (without DMOAP coating) were then immersed in the 5CB LC. Under the same applied temperature gradient of *1°C/mm*, negative thermophoresis was observed with colloidal particles moving from low to high temperature. Furthermore, the particle velocities were greater in higher temperature regions. The data is shown in Fig 1e and Table 1.

Table 1 Velocities of uncoated 5µm Silica colloids in isotropic and anisotropic media

Medium	Temperature	Velocity
85% Glycol	26°C	5.8µm/hr
5CB	26°C	-4.1µm/hr
5CB	30°C	-13.7µm/hr

3.2 Thermophoresis of 5µm Particles in the Nematic LC

Homeotropic anchoring of 5CB at the DMOAP interface was verified by observing the bipolar hedgehog defects or the quadrupolar Saturn rings around the 5µm colloidal particles. Since hedgehog defects are a common feature of strong anchoring of the LC molecules on the surface, we selected colloidal particles that exhibited these topologies. To eliminate defect position as a possible variable, we also focused on dipolar colloids where the accompanying hyperbolic hedgehog defect was on the colder side of the particle (+x direction). A temperature gradient of *3°C/mm* was induced through the LC.

Fig 2b presents exemplary trajectory segments that were used for calculating the mean velocities. There is a drift along the *y*-axis, which we attribute to the small variations of the temperature (see the temperature bump in Fig 1c). Using the temperature dependence on data shown in Fig 1d, we correlated the particle position in the sample to the local temperature.

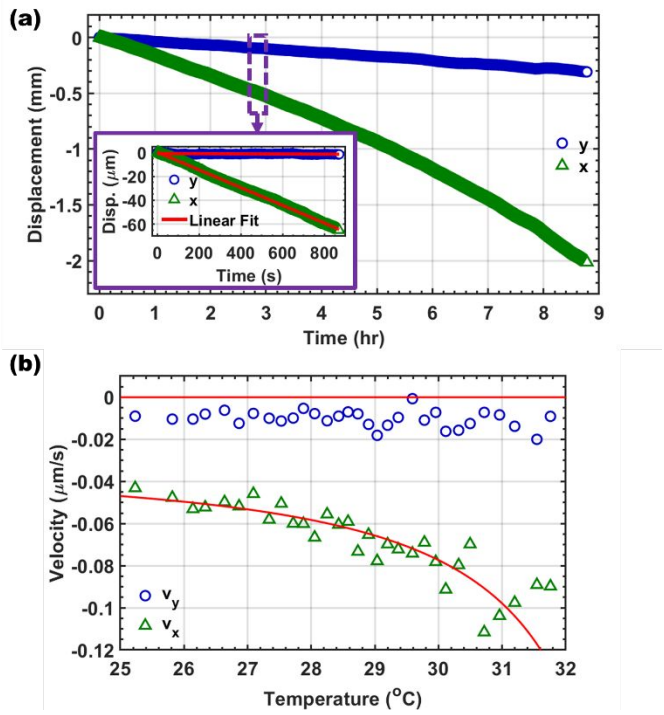

Figure 2 5µm colloid data set. (a) The colloid trajectory stitched together from individual data sets showing nonlinear behaviour. For each individual data set, linear regression was used to fit the local velocity (purple inset). (b) Local velocity of each data set plotted against the average local temperature, which is determined from the average colloid position in each data set using the chart shown in Fig 1d.

3.3 Thermophoresis of 1.6 µm Particles in the Nematic LC

In order to observe positive thermophoresis, we looked to reduce the elastic energy cost of the colloid. Since the elastic energy cost of a colloid in LC scales linearly with size, we used smaller silica colloids (1.6µm diameter) and also reduced the temperature gradient to 1×10^{-4}°C/μm. The resulting colloid velocities were in the order of µm/hr, which meant that up to three colloids in each frame were followed for at least two hours to get an accurate velocity.

In this setup, we were able to observe both positive and negative thermophoresis of colloids in the LC, which is shown in Fig 3. Limitations of the optical resolution in our system made it impossible to get reliable data on motion along the *y*-axis.

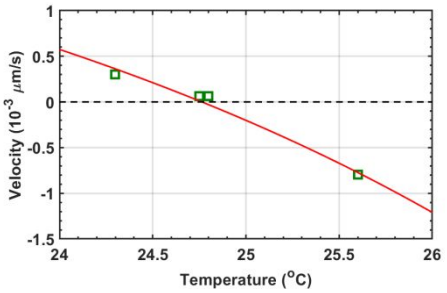

Figure 3 1.6μm colloid data set. The velocity of 1.6μm silica colloids in 5cb calculated over a span of 2 hours using least squares fitting. There is a clear distinction in the cell between colloids above and below 25°C, where motion is dominated by negative and positive thermophoresis, respectively.

4 Theory

Nematic LC is comprised of aligned molecules that exhibit an elastic response to deformation, which can be characterized by an elastic constant, *K*. The elastic energy cost due to the LC director distortion induced by the colloidal particle can be expressed in the integral form of Frank elastic energy.[21,22] The minimization of this Frank energy is a highly non-linear problem, and therefore, it is not usually possible to obtain analytical expressions for the director field around the particle.[39] In the case of rigidly homeotropic anchoring at the surface of the particles and under the single elastic constant approximation, it is possible to make simple arguments to show that the elastic free energy due to the particle scales linearly with the particle radius *R*, $f = 13KR$.[22]

The anchoring energy of 5CB on the self-assembled monolayer of DMOAP is $10^{-2} N/m$, which is considered rigid anchoring.[40] It is therefore reasonable to assume that the elastic energy for the colloid particle is:

$$f = c_e K R \tag{1}$$

where the unitless pre-factor c_e is on the order of 10. Theoretical analysis by Kimura[41] established that the elastic constant of a nematic LC is proportional to the square of the LC order parameter S: $K = K_0 S^2$. The order parameter is related to the temperature *T* through $S = (1 - T/T^*)^{\alpha}$, where *T** is the nematic-isotropic transition temperature. This relation yields

$$K = K_0 \left(1 - \frac{T}{T^*}\right)^{2\alpha} \tag{2}$$

Due to this temperature dependence, a gradient of the elastic energy arises when a temperature gradient dT/dx is present, and the particle experiences an effective force. The total thermophoretic force F acting on the particle is the sum of the traditional thermophoretic force F_t and the effective elastic force $-\partial f/\partial x$:

$$F = F_t - \frac{2\alpha c_e K_0 R dT}{T^* \quad dx}\left(1 - \frac{T}{T^*}\right)^{2\alpha - 1} \tag{3}$$

The drift velocity of the particle can then be obtained from the Stokes law: $v = F/6\pi\eta R$. Using the Stokes-Einstein relation for the diffusion coefficient, $D = k_B T/6\pi\eta R$, the thermophoretic velocity in nematic LCs can be expressed as:

$$v = \frac{D}{k_B T}\left[F_t - \frac{2\alpha c_e K_0 R dT}{T^* \quad dx}\left(1 - \frac{T}{T^*}\right)^{2\alpha - 1}\right] \tag{4}$$

The thermal diffusion coefficient, $D_T \equiv v/\nabla T$, can be written as

$$D_T = D_{T,t} - \frac{2\alpha c_e K_0 R}{T^*}\left(1 - \frac{T}{T^*}\right)^{2\alpha - 1} \tag{5}$$

where $D_{T,t}$ is the thermal diffusion coefficient that results from traditional themophoretic processes in isotropic media. These expression are valid when $T < T^*$.

5 Discussion

5.1 Effective Viscosity

From the 5μm colloid trajectories, we utilized the mean squared displacement ($MSD = 2Dt + v^2 t^2$) to calculate the diffusion constant, D. The effective viscosity of the fluid, η, can be derived from D using Einstein's relation. We could not perform the same calculations on the 1.6μm particles due to a lack of resolution in the optical setup.

In the case of LC, the viscosity of the fluid is increased by the elastic response to director deformation, as shear motion inherently causes reorientation of LC molecules in certain geometries. The geometric conditions are quantified by the Miesowicz viscosities[42] η_1, η_2 and η_3, which describe the viscosity of the fluid in the three orthogonal directions to the LC director (Fig 4a-c). The alignment of the cell necessitates that the motion is broken down into motion parallel (*x*) and perpendicular (*y*) to the director, which experiences bulk viscosities $\eta_b = \eta_2$ and $\eta_b = \eta_1$, respectively (Fig 4d). Due to strong anchoring, the LC at the surface of the colloid is homeotropically aligned (Fig 4d inset), and the local effective (surface) viscosity is $\eta_s = (\eta_1 + \eta_2 + \eta_3)/3$. The total viscosity is a weighted average of surface and bulk viscosities.

When the data collected in this work are overlaid with published Miesowicz viscosities for 5CB[43] (Figure 4e), these characteristics become evident. Perpendicular to the motion and orthogonal to the particle-defect axis, the data show $\eta_1 > \eta_y > \eta_2, \eta_3$, which is consistent with strong LC alignment around the particle biased toward η_1 by the

cell alignment. The relation between the measured viscosity and the individual Miesowicz viscosities has a temperature dependence, wherein η_s decreases from 75% of the total viscosity at 25°C to 45% of the total viscosity at 32°C (blue points in Fig 4f).

Parallel to the motion and along the particle-defect axis, the viscosity is consistent with LC alignment around the particle biased by the alignment in the cell to favour η_2 at lower temperatures. However, the η_2 component becomes completely dominant as the temperature increases. As a function of temperature, the contribution of η_s to the total viscosity decreases from 55% at 25°C to 0% at 32°C (green points in Fig 4f).

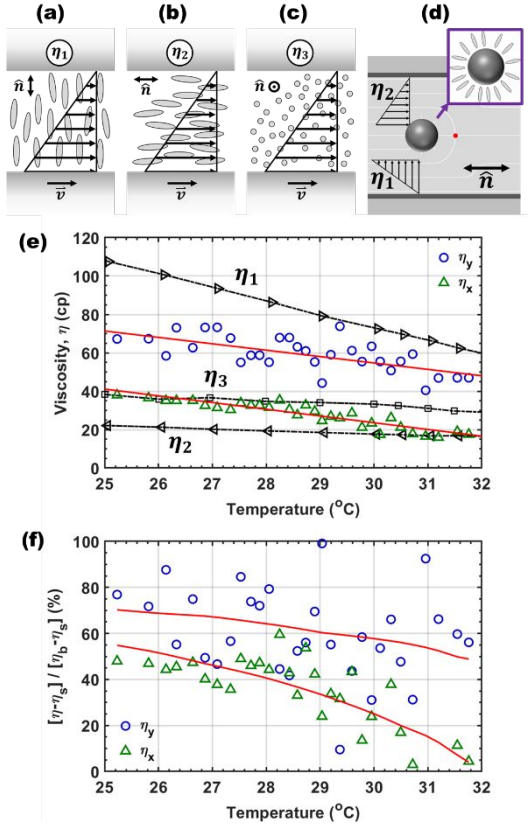

Figure 4 Viscosity of 5μm colloids in 5CB. (a-c) The Miesowicz viscosities of a nematic LC. (d) The director orientation in the cell and around the colloid (purple inset). (e) Viscosity data showing the effective viscosity of the 5μm colloids with relation to the Miesowicz viscosities in the literature[43] (shown in black). Red curves show the linear fit of the data. (f) The contribution of the surface viscosity (taken from literature), η_s, to the measured effective viscosity of the colloid as a function of the temperature. The red curves are calculated using the linear fits of the viscosities shown in red in (e).

Since the system is in the low Ericksen number regime ($Er = \eta v R/K \sim 0.0004 \ll 1$), the velocity of the colloid does not affect the director field[21]. The velocity where the Ericksen number crosses unity is $v_\infty \sim 20\mu m/s$. We can also consider the negative temperature dependence of the surface anchoring energy[44–46], but this a critical phenomenon and does not result in any appreciable variation more than 3°C from the transition temperature.

As a result, the reduction in the surface contribution to the viscosity must be a phenomenon inherent to the energy minimization of the colloid in the LC.

5.2 Thermophoretic Forces

Using F_t and c_e as fitting parameters and a linear approximation for the local viscosity (red lines in Fig 4e), we compared Eq 4 with the measured colloidal velocities in our experiments to obtain good agreement, as is shown in Fig 5. The best fit value of $c_e = 3.9$ is the same order of magnitude as the value of $c_e = 13$ that was theoretically derived for the case of a Saturn ring defect around a colloid[39]. This is consistent with expectations given that a hedgehog defect, which is emblematic of strong surface anchoring, would result in a higher energy cost. An interesting result is that $F_t < 0$, meaning that the traditional thermophoretic force is negative.

To elucidate this behaviour we analysed the first approximation for our system in an isotropic state, neglecting the effects of ionic impurities and solvation entropy. In Brenner's model of thermophoresis in isotropic fluids[2], the thermal diffusion coefficient is defined by taking into account the thermal conductivities of the particle and liquid κ_p and κ_l, as well as the thermal expansion coefficient β, density ρ and the heat capacity c of the liquid. In the case of 5CB, the values approximated from the literature and are shown in Table 2.

Table 2 System Properties

Property	Value	Units	Reference
$\kappa_{l,\|\|}$	0.15	$WK^{-1}m^{-1}$	47,48
κ_P	1.4	$WK^{-1}m^{-1}$	data sheet
β	7.8×10^{-4}	K^{-1}	49
ρ	1.01	$g\ cm^{-3}$	50,51
c	1.9	$Jg^{-1}K^{-1}$	52

LC density has a very weak dependence on temperature, decreasing by less than $0.1\%/°C$ over the range of the study. The thermal conductivity of 5CB exhibits a similarly weak temperature dependence. The thermal expansion coefficient was approximated as that of the cyanobiphenyl mixture E7, since 5CB was not found directly in the literature. The specific heat of 5CB has a stronger pre-transitional effect, ranging from 1.9J/gK at 32°C to 2.4J/gK at the transition around 35°C but varies by less than 5% between 25 and 32°C.

Using the values from Table 1, Brenner's model predicts that the thermal diffusion coefficient is

$$D_{T,t} = \frac{\kappa_l \beta}{\rho c\left(1 + \kappa_p/2\kappa_l\right)} = 11\mu m^2/sK \qquad (6)$$

, which is independent of colloid size. Using Eq 5 with $D_{T,t}$ as a fitting parameter, it is empirically determined that $D_{T,t} = -11\mu m^2/sK$ for the 5μm colloids. Fitting the velocity for the 1.6μm colloids yields $D_{T,t} = 54\mu m^2/sK$ and $c_e = 44$.

A consequence of Eq 4 is the definition of a zero-velocity temperature T^c, where the direction of motion reverses. This is the point at which traditional thermophoretic forces are perfectly balanced by the elastophoretic contribution of the LC. This crossover is not observed in the case of 5μm colloids, but for 1.6μm colloids we observe $T^c = 24.8$℃. From the zero-velocity temperature, we can determine the effective positive thermophoretic force F_t for the 1.6μm colloids to be

$$F_t = \frac{2\alpha c_e K_0 R dT}{T^* \quad dy}\left(1 - \frac{T^c}{T^*}\right)^{2\alpha - 1} = 29fN \qquad (7)$$

Our results suggest that the primary thermophoretic driving force acting on colloidal particles in a nematic LC system at low Ericksen number is the elastic energy minimization of the medium. It is relevant to note that moving colloids with elastic gradients has been widely demonstrated in liquid crystals[21–23,27,53] and even has some analogs in non-liquid crystal systems, such as durotaxis in non-living systems[54].

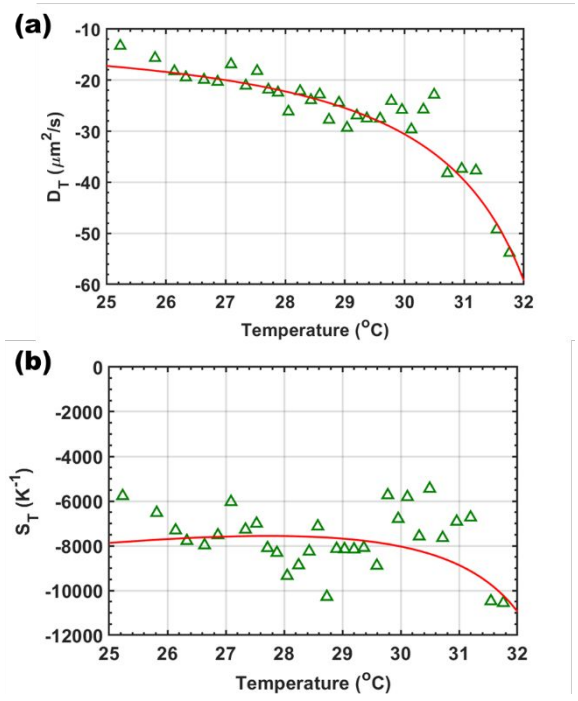

Figure 5 Thermophoretic quantities for 5μm colloids in 5CB. The (a) thermal diffusion coefficient and (b) Soret Coefficient calculated for each data set with a theoretical fit shown in red.

5.3 The Soret Coefficient

The Soret coefficient is the ratio of deterministic to stochastic motion in a temperature gradient and is calculated through the relation $S_T = D_T/D$. This quotient collected for each data point, as well as the ratio of the theoretical fits, is shown in Fig 5. The average value in our measured range is $S_T = -(7.7 \pm 1.3) \times 10^3 K^{-1}$, which is five orders of magnitude higher than isotropic systems reported in literature[55] ($|S_T| \sim 10^{-3} - 10^{-2} K^{-1}$). The significance of this large magnitude is that the thermally induced motion can be easily distinguished from diffusion. The reason for this enhancement is the elastic nature of LC systems: the order parameter of the nematic medium inherently increases the thermophoretic force due to an additional elastophoretic term while simultaneously inhibiting diffusion by elastically resisting deformation.

In sorting applications, a large Soret coefficient greatly reduces the time required to separate two species. However, in LC media this is complicated by the strong interactions between colloidal particles, which leads to self-assembly of complex structures[56–59]. Microfluidic methods of sorting, in which colloids can be isolated, are currently more suited to such techniques[60].

Using the Soret Coefficient, we can infer the operant mechanism behind thermophoresis in our system. Considering $R|S_T|\nabla T \sim 54 > 1$, we can assert that the particle moves by hydrodynamically-based mechanical motion[6]. However, our theory approximates a local isotropic environment to simply the model. Since the model relies on energy minimization and not Marangoni effects, averaging the local anisotropic environment to get an average energy cost is a reasonable assumption.

6 Conclusions

To summarize, we quantified thermophoresis of colloids in nematic LCs and showed that it exhibits salient behaviours: (1) thermophoresis can be negative and very strong, as compared to the phenomenon reported in isotropic systems; (2) as the local temperature increased, there is a nonlinear increase of the thermophoretic velocity; (3) a crossover from negative to positive thermophoresis is possible as one moves down the temperature gradient and traditional thermophoretic forces outweigh elastophoretic contributions. We also presented a theoretical framework for understanding thermophoretic mechanisms in LC systems by incorporating elastic energy considerations into a traditional description of thermophoresis and showed good agreement with experimental results. We analysed the trajectory data to show the effect of temperature on the viscosity of the colloids and thermophoretic force. Finally, we examined the deterministic nature of thermophoretic motion and found a huge enhancement of the Soret coefficient due to a suppression of the diffusion constant and enhancement of the thermophoretic force due to elastophoretic contributions, which are inherent to LC media. From our theoretical foundation, the gradient in order parameter does not have to be inherent from a temperature gradient. Order parameter gradients formed via other methods[61] can be utilized in a similar manner.

Acknowledgements

Acknowledgment is made to the Donors of the American Chemical Society Petroleum Research Fund for support of this research. The authors (JK and QHW) like to acknowledge Taras Turiv and Israel Lazo Martinez for their kind help in the preparing colloidal liquid crystal samples and Oleg D. Lavrentovich for valuable discussions.

References

1 F. Zheng, *Adv. Colloid Interface Sci.*, 2002, **97**, 255–278.
2 H. Brenner, *Phys. A Stat. Mech. its Appl.*, 2005, **349**, 60–132.
3 S. Duhr and D. Braun, *Proc. Natl. Acad. Sci. U. S. A.*, 2006, **103**, 19678–82.
4 M. Reichl, M. Herzog, A. Gotz, D. Braun, A. Götz and D. Braun, *Phys. Rev. Lett.*, 2014, **112**, 198101.
5 D. Vigolo, S. Buzzaccaro and R. Piazza, *Langmuir*, 2010, **26**, 7792–801.
6 R. D. Astumian, *Proc. Natl. Acad. Sci.*, 2007, **104**, 3–4.
7 H. Brenner, *Phys. Rev. E. Stat. Nonlin. Soft Matter Phys.*, 2006, **74**, 036306.
8 B. J. De Gans, R. Kita, B. Müller and S. Wiegand, *J. Chem. Phys.*, 2003, **118**, 8073–8081.
9 R. Kita, S. Wiegand and J. Luettmer-Strathmann, *J. Chem. Phys.*, 2004, **121**, 3874–3885.
10 S. Iacopini and R. Piazza, *Europhys. Lett.*, 2007, **63**, 247–253.
11 R. Piazza and A. Parola, *J. Phys. Condens. Matter*.
12 J. Burelbach, D. Frenkel, I. Pagonabarraga and E. Eiser, *Eur. Phys. J. E*, , DOI:10.1140/epje/i2018-11610-3.
13 F. A. Messaud, R. D. Sanderson, J. R. Runyon, T. Otte, H. Pasch and S. K. R. Williams, *Prog. Polym. Sci.*, 2009, 34, 351–368.
14 G. Liu and J. C. Giddings, *Chromatographia*, 1992, **34**, 483–492.
15 J. Giddings, *Science (80-.).*, 1993, **260**, 1456–1465.
16 M. Jerabek-Willemsen, T. André, R. Wanner, H. M. Roth, S. Duhr, P. Baaske and D. Breitsprecher, *J. Mol. Struct.*, 2014, **1077**, 101–113.
17 C. J. Wienken, P. Baaske, U. Rothbauer, D. Braun and S. Duhr, *Nat. Commun.*, 2010, **1**, 100.
18 M. Jerabek-Willemsen, C. J. Wienken, D. Braun, P. Baaske and S. Duhr, *Assay Drug Dev. Technol.*, 2011, **9**, 342–53.
19 R. Di Leonardo, F. Ianni and G. Ruocco, *Langmuir*, 2009, **25**, 4247–50.
20 D. Vigolo, R. Rusconi, H. A. Stone and R. Piazza, *Soft Matter*, 2010, **6**, 3489.
21 H. Stark, *Phys. Rep.*, 2001, **351**, 387–474.
22 O. D. Lavrentovich, *Soft Matter*, 2014, **10**, 1264–83.
23 M. A. Gharbi, M. Nobili, M. In, G. Prévot, P. Galatola, J.-B. Fournier and C. Blanc, *Soft Matter*, 2011, **7**, 1467–1471.
24 J. C. Loudet, P. Hanusse and P. Poulin, *Science*, 2004, **306**, 1525.
25 A. C. Diogo, *Mol. Cryst. Liq. Cryst.*, 2011, **100**, 153–165.
26 R. W. Ruhwandl and E. M. Terentjev, *Phys. Rev. E*, 1996, **54**, 5204–5210.
27 H. Stark and D. Ventzki, *Phys. Rev. E. Stat. Nonlin. Soft Matter Phys.*, 2001, **64**, 031711.
28 J. B. Rovner, D. H. Reich and R. L. Leheny, *Langmuir*, 2013, **29**, 2104–7.
29 H. Stark and D. Ventzki, *Europhys. Lett.*, 2002, **57**, 60–66.
30 H. Stark, D. Ventzki and M. Reichert, *J. Phys. Condens. Matter*, 2003, **15**, S191–S196.
31 A. V. Ryzhkova, F. V. Podgornov and W. Haase, *Appl. Phys. Lett.*, 2010, **96**, 151901.
32 O. D. Lavrentovich, I. Lazo and O. P. Pishnyak, *Nature*, 2010, **467**, 947–50.
33 M. Skarabot, M. Ravnik, D. Babic, N. Osterman, I. Poberaj, S. Zumer, I. Musevic, A. Nych, U. Ognysta and V. Nazarenko, *Phys. Rev. E. Stat. Nonlin. Soft Matter Phys.*, 2006, **73**, 021705.
34 I. Musevic, M. Skarabot, D. Babic, N. Osterman, I. Poberaj, V. Nazarenko and A. Nych, *Phys. Rev. Lett.*, 2004, **93**, 187801.
35 B. Lev, A. Nych, U. Ognysta, S. B. Chernyshuk, V. Nazarenko, M. Skarabot, I. Poberaj, D. Babic, N. Osterman and I. Musevic, *Eur. Phys. J. E. Soft Matter*, 2006, **20**, 215–9.
36 S. A. Tatarkova, D. R. Burnham, A. K. Kirby, G. D. Love and E. M. Terentjev, *Phys. Rev. Lett.*, 2007, **98**, 157801.
37 M. Škarabot, Ž. Lokar and I. Muševič, *Phys. Rev. E. Stat. Nonlin. Soft Matter Phys.*, 2013, **87**, 062501.
38 N.-S. Cheng, *Ind. Eng. Chem. Res.*, 2008, **47**, 3285–3288.
39 O. V. Kuksenok, R. W. Ruhwandl, S. V. Shiyanovskii and E. M. Terentjev, *Phys. Rev. E*, 1996, **54**, 5198–5203.
40 M. Skarabot, M. Ravnik, S. Zumer, U. Tkalec, I. Poberaj, D. Babic and I. Musevic, *Phys. Rev. E. Stat. Nonlin. Soft Matter Phys.*, 2008, **77**, 061706.
41 H. Kimura, M. Hosino and H. Nakano, *Mol. Cryst. Liq. Cryst.*, 1981, **74**, 55–69.
42 M. Miesowicz, *Nature*, 1946, **158**, 27.
43 M. Cui and J. R. Kelly, *Mol. Cryst. Liq. Cryst. Sci. Technol. Sect. A. Mol. Cryst. Liq. Cryst.*, 1999, **331**, 49–57.
44 P. Chiarelli, S. Faetti and L. Fronzoni, *Phys. Lett. A*, 1984, **101**, 31–34.
45 H. Yokoyama, S. Kobayashi and H. Kamei, *J. Appl. Phys.*, 1987, **61**, 4501.
46 H. Yokoyama, S. Kobayashi and H. Kamei, *J. Appl. Phys.*, , DOI:10.1063/1.323928.
47 M. Marinelli, F. Mercuri, U. Zammit and F. Scudieri, .
48 G. Ahlers, D. S. Cannell, L. I. Berge and S. Sakurai, *Phys. Rev. E*.

49 Y.-K. Kim, B. Senyuk and O. D. Lavrentovich, *Nat. Commun.*, 2012, **3**, 1133.
50 G. A. Oweimreen, A. K. Shihab, K. Halhouli and S. F. Sikander, *Mol. Cryst. Liq. Cryst.*, 1986, **138**, 327–338.
51 J. Deschamps, J. P. M. Trusler and G. Jackson, *J. Phys. Chem. B*, 2008, **112**, 3918–26.
52 G. S. Iannacchione and D. Finotello, *Phys. Rev. E*, 1994, **50**, 4780–4795.
53 I. Muševič, M. Škarabot, U. U. Tkalec, M. Ravnik, S. Žumer, I. Musevic, M. Skarabot, U. U. Tkalec, M. Ravnik and S. Zumer, *Science*, 2006, **313**, 954–8.
54 R. W. Style, Y. Che, S. J. Park, B. M. Weon, J. H. Je, C. Hyland, G. K. German, M. P. Power, L. A. Wilen, J. S. Wettlaufer and E. R. Dufresne, *Proc. Natl. Acad. Sci. U. S. A.*, 2013, **110**, 12541–4.
55 J. K. Platten, *J. Appl. Mech.*, 2006, **73**, 5–15.
56 I. Muševič and M. Škarabot, *Soft Matter*, 2008, **4**, 195–199.
57 T. Kishita, K. Takahashi, M. Ichikawa, J. Fukuda and Y. Kimura, *Phys. Rev. E. Stat. Nonlin. Soft Matter Phys.*, 2010, **81**, 010701.
58 K. Takahashi, M. Ichikawa and Y. Kimura, *J. Phys. Condens. Matter*, 2008, **20**, 75106–5.
59 I. I. Smalyukh, O. D. Lavrentovich, A. N. Kuzmin, A. V Kachynski and P. N. Prasad, *Phys. Rev. Lett.*, 2005, **95**, 157801.
60 A. Sengupta, S. Herminghaus and C. Bahr, *Liq. Cryst. Rev.*, 2014.
61 S. Samitsu, Y. Takanishi and J. Yamamoto, *Nat. Mater.*, 2010, **9**, 816–20.

Colloids in Liquid Crystal media with an applied temperature gradient exhibit strong thermophoretic motion due to temperature-dependent elastic forces.